Dynamics of β_1-Integrins in Living Fibroblasts—Effect of Substratum Wettability

I. Zlatanov,* T. Groth,[†‡] A. Lendlein,[‡] and G. Altankov*[‡]
*Institute of Biophysics, Bulgarian Academy of Sciences, Sofia, Bulgaria; [†]Biomedical Materials, Institute of Bioengineering, Martin-Luther University, Halle-Wittenberg, Halle, Germany; and [‡]GKSS Research Center, Institute of Chemistry, Teltow, Germany

ABSTRACT The dynamics of integrin receptors mobility was studied in living human fibroblasts using fluorescence-labeled β_1-integrin monoclonal antibodies. Time-lapse image series were obtained by confocal laser scanning microscopy when cells were adhering on model hydrophilic (clean glass) and hydrophobic (octadecyl-silanized; i.e., ODS) surfaces coated with fibronectin. Direct measurements showed approximately twice-higher velocity of integrins on glass compared to ODS, and these velocities varied in different zones of the cells. A kinetic model and algorithm for quantification of images was developed, and the analysis identified three receptor populations on glass: immobilized (82.76% of all), slow (4.16%), and fast (13.08%), while, on ODS, only two were identified: immobilized (83.36%) and fast (16.64%). Fast integrins in the peripheral zone of cells have maximal velocities of 0.353 ± 0.02 μm/min ($n = 48$, four cells) on hydrophilic and 0.218 ± 0.02 μm/min ($n = 30$, three cells) on hydrophobic substrata. The slow population has a velocity of 0.114 μm/min ($n = 48$, four cells). Further analyses show that these velocities also differ significantly in the peripheral and middle zones of cells in a substrate-dependent fashion. A well-defined circular motion of receptors around the cell center expressed mainly on hydrophobic substrata was monitored and quantified as well.

INTRODUCTION

Integrin receptors play a crucial role for the interaction of cells with the extracellular matrix regulating their adhesion, migration, proliferation, and survival (1,2). It has been also recognized that integrins are important regulators of cellular behavior on foreign material surfaces (1,3,4). Integrins recognize matrix proteins such as fibronectin (FN) adsorbed on material surfaces in a conformation-dependent manner, which, in turn, is strongly dependent of the physical and chemical composition of the substrata (5,6,7). Wettability is one parameter in particular that strongly influences the conformation of adsorbed FN, which governs the subsequent cellular interaction (5). In quiescent fibroblasts, integrins concentrate in focal adhesions (2,6,8,9), which are specialized adhesion sites that anchor stress fibers and provide cultured cells with firm substrate attachments (2,6). When fibroblasts adhere on FN, they develop a second type of structure, named *extracellular matrix contacts* (10), which have been recently renamed *fibrillar adhesions* (11,12). In contrast to focal contacts, fibrillar adhesions bind extracellular fibrils of FN parallel to actin bundles, and their function seems to be critical for the organization of FN matrix (12).

Most of our current knowledge on the above-mentioned adhesive structures is based on biochemical studies and morphological observations of fixed cells. Recently, however, there have been several investigations on integrin dynamics (12–15) that provide significant insight into the functioning of these unique receptors. Smilenov et al. (13) have first shown that certain focal contacts, visualized by GFP-labeled β_1-integrin, are able to move centripetally in nonmotile fibroblasts with a velocity of 0.12 ± 0.08 μm/min. Further studies demonstrated that fibrillar adhesions originate from the peripheral focal contacts, from where they segregate centripetally (12). Fibrillar adhesions contain the main FN receptor $\alpha_5\beta_1$-integrin, while $\alpha_v\beta_3$ remains located in focal contacts (6,12,14). There were various attempts for measuring the velocity of integrins. The method of fluorescence recovery after photobleaching has been applied by Duband et al. (16) and the lateral diffusion coefficients of integrin clusters were estimated to be in the range of 2×10^{-10} to 4×10^{-10} cm^2/s in avian embryonic cells, which is equal to velocities of 0.2 to 0.4 μm/min. With similar technique, Palecek et al. (17) have measured integrin velocity in chicken myofibroblasts ranging from 0.017 to 1.33 μm/min. Using image correlation microscopy, Wiseman et al. (18) provide us with unique information about the density, dynamics, and interaction of α_5-integrins in migrating CHO cells. They show that α_5-YFP integrins are usually present in submicroscopic clusters containing 3–4 integrins, which further develop in nascent adhesions. In more mature adhesions where the integrins are visibly organized, there are already ~900 integrins per μm^{-2}. Conversely, during adhesion disassembly the integrins diffuse away from adhesions with ~0.29 μm min^{-1}, a speed similar to actin retrograde flow. Some authors have used antibodies to investigate the integrin dynamics. Kawakami et al. (19) using time-lapsed total-internal-reflection fluorescence microscopy estimated the velocity of β_1-integrin-antibody complex of $\sim 0.29 \pm 0.24$ μm/min for vein endothelial cells. It is widely accepted that binding of anti-integrin antibodies may mimic, to a certain extent, their physiological occupation by ligand (20,21). Moreover, the antibody tagging may activate integrins provoking their

Submitted February 14, 2005, and accepted for publication July 6, 2005.

Address reprint requests to G. P. Altankov, Tel.: 359-2-979-2634; E-mail: altankov@obzor.bio21.bas.bg.

0006-3495/05/11/3555/08 $2.00

doi: 10.1529/biophysj.105.061119

clustering and reorganization, thus working as an instrument to visualize their functional behavior (22–24).

Most quantitative measurements of integrin dynamics, however, were performed when cells spread on standard tissue culture substrata, whereas data on the impact of material surface properties, such as wettability or surface chemistry, are almost missing. Some times ago, using human fibroblasts adhering on model hydrophilic and hydrophobic surfaces coated with FN, we have shown that the wettability of the substratum is an important factor for the β_1-integrin functioning and organization (3,25,26). We showed that signaling of integrins via tyrosine phosphorylation in focal contacts is blocked on hydrophobic ODS (25) and other poorly wettable substrata (27). Other authors clearly show that surface chemistry also modulates focal adhesion composition and signaling (7). The same was found for FN reorganization, which is another important parameter for the assessment of biocompatibility of materials (26,28,29). Moreover, it corresponded to the aberrant organization of β_1-integrin antibody complex on hydrophobic surfaces (29).

Here, with fibroblasts adhering on model hydrophilic (glass) and hydrophobic (ODS) surfaces, we show that the previously observed impaired integrin function on hydrophobic surfaces is related to differences in β_1-integrin dynamics. Tagging β_1-integrins with FITC-labeled monoclonal antibodies, we followed their fate in time-lapse image series with confocal laser scanning microscopy (CLSM). In addition to direct measurements of integrin velocities, a kinetic model for integrin density dynamics, measured at different cell regions, was developed. The analysis unpredictably identified three receptor populations that differ in their velocities and cellular distribution in a substratum-dependent manner. Details of this investigation and the algorithm for quantification of images are presented below.

MATERIALS AND METHODS

Cells

Human fibroblasts were obtained from fresh skin biopsies and used up to the 10th passage. Cells were grown in Dulbecco's modified Eagle's medium (DMEM) containing 10% fetal calf serum (FCS) (Sigma-Aldrich, St. Louis, MO) in a humidified incubator with 5% CO_2. Fibroblasts from preconfluent cultures were harvested with 0.05% trypsin/0.6 mM EDTA (Sigma-Aldrich). Trypsin was neutralized with FCS.

Preparation of model hydrophilic and hydrophobic surfaces

Clean round microscopic glass slides of 35-mm diameter (PeCon, Erbach-Buch, Jena, Germany) were cleaned with ethanol and phosphate-buffered saline (PBS) containing 150 mM NaCl, 5.8 mM Na_2HPO_4, and 5.8 mM NaH_2PO_4. They were used as model hydrophilic surfaces. The water contact angles (WCA) were estimated by the sessile drop method. The WCA of clean glass was $25° \pm 2.7°$, which indicated a relatively hydrophilic surface. To render the surface hydrophobic, the slides were cleaned with Piranha solution (3:1 concentrated sulphuric acid and 33% hydrogen peroxide). They were silanized by immersion in 1 mg/ml octadecyldimethylchlorosilane (ODS, Sigma-Aldrich) dissolved in chloroform as previously described (26,28). The WCA of ODS was $87° \pm 1.7°$, indicating a hydrophobic surface.

Fluorescent staining of integrins in living fibroblasts

Standard silicon cell culture chambers (FlexiPerm, Vivascience, Hanau, Germany) were attached to the glass slides. The resulting surfaces at the bottom of chambers were washed before use with PBS, then coated with 20 μg/ml fibronectin (FN) in PBS at room temperature for 30 min, and subsequently washed with PBS and DMEM. Approximately 6×10^3 fibroblasts in 450-μl serum-free DMEM were added to each chamber and incubated for 1 h in a humidified CO_2 incubator at 37°C to give time for appropriate cell attachment and spreading. The samples were cooled to 4°C for 10 min and incubated for 10 min with an FITC-conjugated anti-β_1-integrin monoclonal antibody (CD29, Cat. No. 2908; Biosource International, Camarillo, CA), diluted 1:50 in 100-μl DMEM containing 10% FN-free FCS. Beforehand, the FN was removed from the serum by gelatin-Sepharose 4B (Pharmacia, Uppsala, Sweden). The cells were then washed three times with DMEM to remove the nonbound antibody, and immersed in 450-μl DMEM containing 10% FN-free FCS.

Confocal laser scanning microscopy and image analysis

Time-lapse microscopy was performed with a confocal laser scanning microscope type LSM 510 (Carl Zeiss, Jena, Germany) equipped with thermostatic chamber type Temp-Control 37-2 (PeCon). The latter was fitted to the microscope stage. The glass slides and the attached silicon chamber were placed inside. The temperature at the bottom of the sample was precisely adjusted to 37°C by a calibrated thermocouple. Single cells were scanned every 10 min using the automated time-lapse series mode up to 2.5 h.

Image sequences were exported by the LSM Image Examiner software (Carl Zeiss) in TIFF format and captured on the hard drive in separate folders. Due to cellular movements, some images in a series were out of focus; these images were discarded. The remaining images in the sequences were processed and analyzed by the freely available Java-based public domain software ImageJ, Vers. 1.32a, developed at the National Institutes of Health, Bethesda, MD (http://rsb.info.nih.gov/ij/). Using the Region of Interest Manager and the Freehand selection tool of this program, it is possible to specify different regions of the investigated cell, and then quantify the fluorescence (mean shaded value), area, and standard deviations in each.

Measurement of individual velocities of the integrin clusters

To analyze the behavior of integrins, we applied two approaches: 1), we measured the individual velocities of the integrins; and 2), we measured the dynamic changes in the integral integrin densities indicating the fluorescence of specific areas (described below).

Watching the image sequences referenced above, one can easily recognize single integrin-antibody clusters moving centripetally. We choose an appropriate cluster and measure its velocity, estimating the coordinates on a few consecutive images in a time-lapsed series. Briefly, using the Mark and Count tool of the ImageJ software, we marked the moving particle in one of the time-lapsed pictures and thus obtained the coordinates x_1,y_1 at time t_1. Watching the next picture of the sequence, we marked the same cluster and counted its new coordinates x_2,y_2 at time t_2. Knowing these coordinates, one can calculate the distance between point x_1,y_1 and x_2,y_2 in pixels, and further convert the distances in micrometers using the CLSM Image Examiner tool (Carl Zeiss). Times t_1 and t_2 we also know exactly, from the data of the

image sequence (using the CLSM tools *Gallery* and *Data*). In different cell regions, we measured a sufficient number of clusters (at least 10), as indicated in the text.

The angular velocities were measured with the Measure Angle plug-in of the ImageJ software. For example, the frequency of rotation is

$$\omega = (\alpha_2 - \alpha_1)/(t_2 - t_1)\ \text{in}\ [\text{deg/min}], \tag{1}$$

where α_1 and α_2 are the relative angles at moments t_1 and t_2 when the respective images were made. Thus, the angular velocity of the given cluster is

$$V_a = (\omega \times r)/360\ \text{in}\ [\mu\text{m/min}], \tag{2}$$

where (r) is the radius of the rotation, i.e., the distance between the cluster and its center of rotation.

Measurement of the integrin density and their dynamics

To analyze the mass redistribution and centripetal flow of integrin receptors, we created a model and algorithm for quantification of the image parameters.

Backgrounds and definitions

A part of the fluorescent antibodies binds to β_1-integrins during the labeling procedure. Since nonbound antibody was removed by washing procedures, one can accept that the quantity of bound antibody remains constant during the experiment and is proportional to the number (N) of labeled receptors. Hence, the fluorescence (F) of the whole cell is

$$F = \text{const} \times N. \tag{3}$$

The specific fluorescence is defined as fluorescence (F_{sp}) of a single area (A). Then using Eq. 1, we obtain

$$F_{sp} = F/A = \text{const} \times (N/A). \tag{4}$$

The ratio N/A, however, represents the density of integrin receptors at a defined region of the cell, and thus Eq. 4 gives a direct expression of density by the fluorescence. Both parameters F and A were measured by the Analyze plug-in of ImageJ.

Construction of regions of interest (ROI) and special regions of interest (SROI)

We defined three zones of special region of interest (SROI), well recognized in most of the cells (see Fig. 1); namely, a peripheral zone (PZ), $SROI_1$; a middle zone (MZ), $SROI_2$; and a central or nuclear zone (NZ), $SROI_3$. The ROIs at time t_1 (i.e., the first image of a given cell) were created by the Freehand selection of the ImageJ software, as shown in Fig. 1. ROI_1 includes the entire cell area (marking the contour of the cell); ROI_2, the middle and the nuclear zones; and ROI_3, the nuclear zone only. At each time t_n in the time series the ROIs were defined the same way, and named ROI_1^{tn}, ROI_2^{tn} and ROI_3^{tn}, respectively. The parameters that we measured were the fluorescence, F_m^{tn}($m = 1, 2, 3$ is the number of ROI; $n = 1, 2, 3 \ldots n$ is the number of analyzed images in a time-lapsed series), and the respective area of the cell, A_m^{tn} . Thus, measuring the changes in these parameters with time, we investigated the dynamics of integrin receptor redistribution.

For example, when we analyzed $SROI_1$, i.e., PZ, which covers the space between ROI_1 and ROI_2, we measured the fluorescence of this region at time t_n as $(F_1^{tn} - F_2^{tn})$ and the respective area as $(A_1^{tn} - A_2^{tn})$. The specific fluorescence of this zone is

$$F_{pz}^{sp} = (F_1^{tn} - F_2^{tn})/(A_1^{tn} - A_2^{tn}). \tag{5}$$

To eliminate background fluorescence and other systemic noise, at every time t_n we measured the fluorescence F_b^{tn} and the area A_b^{tn} of a defined segment from the background outside the cell (see the *marked squares* in Fig. 1). Thus, the specific fluorescence of the background is

$$F_b^{sp} = F_b^{tn}/A_b^{tn}, \tag{6}$$

and studying the ratio F_{pz}^{sp}/F_b^{sp} from Eqs. 5 and 6 we obtain a nondimensional signal/noise ratio D_{pz}^{tn}, which is a function of t_n and proportional to the real density of the receptors,

$$D_{pz}^{tn} = \text{const} \times [(F_1^{tn} - F_2^{tn}) \times A_b^{tn}]/[F_b^{tn} \times (A_1^{tn} - A_2^{tn})]. \tag{7}$$

The relation of this density to the initial one at time t_1 is

$$D_{pz}^{tn}/D_{pz}^{t1} = [(F_1^{tn} - F_2^{tn}) \times A_b^{tn}] \times [F_b^1 \times (A_1^1 - A_2^1)]/ (F_1^1 - F_2^1) \times A_b^1] \times [F_b^{tn} \times (A_1^{tn} - A_2^{tn})]. \tag{8}$$

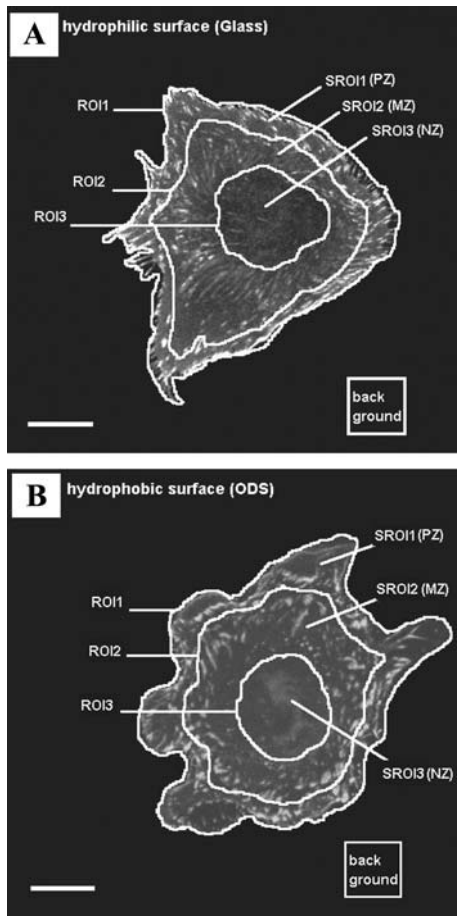

FIGURE 1 Illustration of construction of regions of interest (*ROI*) and special ROI (*SROI*) in fibroblast spread on hydrophilic glass (*A*) and hydrophobic ODS (*B*) substrata. The rectangles that represent distinct part of the background outside the cells have area A_b and fluorescence F_b. First ROI_1 includes all cell area, second (ROI_2), the middle and central (nuclear) zone, and third (ROI_3) includes the nuclear zone only. Areas A_{tn} and fluorescence F_{tn} of these zones were measured at different moments t_n. $SROI_1$ is the band between ROI_1 and ROI_2 that covers the peripheral zone (*PZ*) of the cell. Second band, between ROI_2 and ROI_3, represents $SROI_2$, e.g., the middle zone (*MZ*), while $SROI_3$ coincides with the central nuclear zone (*NZ*). All ROIs were drawn by the Freehand selection tool of the ImageJ software, and fluorescence intensities and areas were also measured by ImageJ. Bars are 20 μm.

For example, when the density in the peripheral zone D_{pz} changes with the time as a result of receptor movement, D_{pz} is, consequently, a function of the time.

If we assume that the initial density is 100% = 1, then from Eq. 8 we obtain

$$D^{tn}_{pz} = \{[(F^{tn}_1 - F^{tn}_2) \times A^{tn}_b] \times [F^1_b \times (A^1_1 - A^1_2)]\} / \{[(F^1_1 - F^1_2) \times A^1_b] \times [F^{tn}_b \times (A^{tn}_1 - A^{tn}_2)]\}. \quad (9)$$

Because all parameters in the right side of this expression are measurable, we are able to plot the obtained kinetics of integrin density in PZ as a relative change to the initial density. The densities for the middle and nuclear zones were obtained by following the same procedure.

Corrections for photobleaching

As we assumed above, the quantity of receptors in the whole cell remains constant during the experiment and the bleaching affects only the fluorescence intensity as a function of the number of scans. Using the specific fluorescence of the first ROI_1 as a base we can define a correction function as

$$K(p) = [F^1_1/A^1_1]/[F^p_1/A^p_1], \quad (10)$$

where F^1_1 and A^1_1 are the fluorescence and the area of the whole cell (ROI_1) at the first scan. F^p_1 and A^p_1 are the fluorescence and area at scan p. Note that the number of scans (p) was sometimes different from the number (m) of individual images because we discarded images that were not focused due to cellular movements. From the experimental protocols, however, we know how many scans were made, as well as the respective time t_n. Hence, we can substitute the argument (p) by time t_n in Eq. 8 to obtain the correction function,

$$K^{tn} = [F^1_1/A^1_1]/[F^{tn}_1/A^{tn}_1]. \quad (11)$$

Then, the correction for bleaching in the peripheral zone (Eq. 9) is

$${}^{corr}D^{tn}_{pz} = K^{tn} \times D^{tn}_{pz}. \quad (12)$$

This correction function is specific for each single cell and was used for the peripheral, middle, and nuclear zones of the same cell. The data for fluorescence and areas of the different regions were then processed with the ORIGIN software. Calculations according to Eq. 12 were performed to plot kinetics and fit experimental curves to different models (exponential or linear functions).

RESULTS

Organization of β_1-integrins

Fibroblasts were spread on glass or ODS coated with FN. After addition of FITC-labeled antibodies, β1-integrins were found to concentrate at cell borders. They were organized as fluorescent streaks, which were slightly longer on glass than on ODS (Fig. 1 *A* versus Fig. 1 *B*). Otherwise, the cells were spread almost equally on both substrata within 2.5 h of the experiments, particularly when substrata were coated with FN (28). Presumably these streaks in PZ represent clusters of focal adhesions, which are accessible for antibodies and are located on the ventral cell surface (see Fig. 1). The MZ contained moderately dense fluorescent particles that were often organized as thin linear structures, particularly when cells adhered on hydrophilic glass. However, they were absent on hydrophobic ODS, which confirmed our previous observation (29). On ODS, β1-integrins were clustered in a rather dotlike pattern (Fig. 1 *B*), but nevertheless, all these structures were found to move centripetally on both glass and ODS. Conversely, NZ, which was usually darker, often represented single integrin clusters that moved chaotically on glass or turned around the cell center on ODS (Supplementary Material available from author upon request).

Direct measurement of integrin velocities

In Table 1 are shown the mean centripetal velocities of integrin clusters measured in PZ and MZ. The velocity on glass was significantly higher ($p < 0.05$), of ~1.6 times for the PZ and ~2.5 times in the MZ, when compared to hydrophobic ODS. There was no significant difference in velocities of integrins between PZ and MZ on ODS, whereas, on glass, integrins had a significantly higher speed in the MZ. However, in the NZ, the centripetal movement was absent. Some of integrin clusters here still moved chaotically on glass, where their speed was approximately twice-faster than on ODS (Table 2). Conversely, on ODS integrins were found to turn mostly around the cell center with a speed that was approximately four-times faster than on glass, when we quantified the angular parameters of such particles (ω and V_a in Table 2).

Dynamics of β_1-integrin density

The dynamic redistribution of β_1-integrin density in living cells upon antibody tagging is presented as a time-lapsed series (available under request).

Following the algorithm described in Materials and Methods and Eq. 12, we studied, altogether, seven movies of four cells on glass and three on ODS. Fig. 2 shows typical results for one cell on glass and one on ODS (Fig. 1, *A* and *B*), and the respective quantitative measurements of the integrin density in three zones PZ, MZ, and NZ, when cells were spread on glass or ODS. In these specific cases, the initial relative densities for the cell on glass were: peripheral zone, ${}^{G}D_{pz} = 0.377$; middle zone, ${}^{G}D_{mz} = 0.542$; and nuclear zone, ${}^{G}D_{nz} = 0.08139$ (${}^{G}D_{pz} + {}^{G}D_{mz} + {}^{G}D_{nz} = 1$). Initial relative densities

TABLE 1 Experimental data of direct measurements of the centripetal velocities of integrin receptors in peripheral zone (PZ) and middle zone (MZ) of fibroblasts, spread on hydrophilic glass and hydrophobic ODS

Velocities in:	Glass	ODS
PZ (in μm/min)	0.353 ± 0.020 (n = 48; 4 cells)	0.218 ± 0.020 (n = 30, 3 cells)
MZ (in μm/min)	0.520 ± 0.030 (n = 44; 4 cells)	0.211 ± 0.016 (n = 35, 3 cells)

Data represent the mean values and the respective standard errors of the mean (means ± SE) at a level of significance $p < 0.05$ and (n) is the number of measured particles. Measurements were made by the tool Mark and Count of the image-analysis software ImageJ, described in Materials and Methods.

TABLE 2 Experimental data of direct measurements of the velocities of integrin receptors in NZ of cells, spread on glass and ODS

Velocity	Glass	ODS	Dimension
Linear movement (chaotic)	0.435 ± 0.04 (n = 37, 4 cells)	0.19 ± 0.026 (n = 30, 3 cells)	μm/min
Angular movement ω = angle/time	0.1 ± 0.008 (n = 34, 4 cells)	0.8 ± 0.08 (n = 30, 3 cells)	°/min
Angular movement $V_a = \omega \times r$	0.007 ± 0.0005 (n = 34, 4 cells)	0.032 ± 0.002 (n = 30, 3 cells)	μm/min

Data represent the mean values and the respective standard errors of the mean (± SE) at level of significance $p < 0.05$; (n) is the number of measured particles. Measurements were provided by the tools Mark and Count and Angle of the image-analysis software ImageJ, described in Materials and Methods. Note that ω is the frequency of rotation, V_a is the angular velocity, and r is the radius (distance between particle and the center of rotation).

for the cell on ODS were: peripheral zone, ${}^{ODS}D_{pz} = 0.3323$; middle zone, ${}^{ODS}D_{mz} = 0.38396$; and nuclear zone, ${}^{ODS}D_{nz} = 0.28689$ (${}^{ODS}D_{pz} + {}^{ODS}D_{mz} + {}^{ODS}D_{pz} = 1$).

Fig. 2 presents the results from the quantitative measurements of integrin densities in the three zones for cells on glass (*asterisk*) and ODS (*open circle*), respectively. As a result of the centripetal movement, integrins from the PZ diminished nonlinearly with time. Fitting kinetic models (exponential functions) to the experimental points (see Fig. 2 *A*, *upper curve*), we obtained that, on hydrophilic glass, density of integrins diminished to an exponential decay of second order,

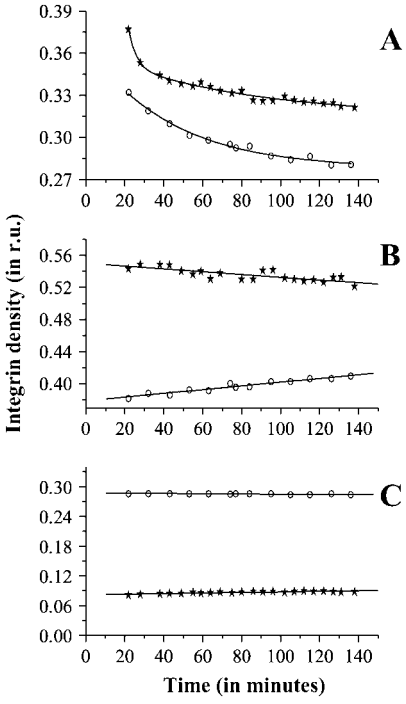

FIGURE 2 Time-dependent changes in the integrin densities at different cell zones. Human fibroblasts were adhered to hydrophilic glass or hydrophobic ODS. The initial densities in relative units for the cell on glass were for peripheral zone $D^G_{PZ} = 0.377$, for middle zone $D^G_{MZ} = 0.542$, and for nuclear zone $D^G_{NZ} = 0.08139 (D^G_{PZ}+D^G_{MZ}+D^G_{NZ} = 1)$; the respective densities for cell on ODS were peripheral zone $D^{ODS}_{PZ} = 0.3323$, middle zone $D^{ODS}_{MZ} = 0.38396$, and nuclear zone $D^{ODS}_{NZ} = 0.28689 (D^{ODS}_{PZ}+D^{ODS}_{MZ}+D^{ODS}_{NZ} = 1)$. The curves in *A* represent the integrin dynamics in PZ of the cell on glass (★) and ODS (○), respectively. *B* presents the data for middle zone of the cells also on glass (★) and ODS (o), and *C* presents dynamics in the central zone. All points are the mean values ± standard error of the means ± SE, which did not exceed 5%.

$$D(t) = D_{min} + D_1 \times \exp(-t/k_1) + D_2 \times \exp(-t/k_2), \quad (13)$$

where $D(t)$ is the density of integrins as a function of time t (in minutes). The values for the constants were as follows: the minimal density at time $t \rightarrow \infty$ is $D_{min} = 0.312 \pm 0.00076$; $D_1 = 0.066 \pm 0.0039$; $D_2 = 0.021 \pm 0.002$; $k_1 = 32 \pm 3$; and $k_2 = 98.5 \pm 9.8$.

In terms of the classical kinetics, Eq.13 represents three populations of particles. First, there are immobile integrins with a density $D_{min} = 0.312 \pm 0.00076$. Having in mind that the initial density of integrins in PZ is $D(t_0) = 0.377 \pm 0.004$ (Fig. 1 *A*), the relative part of immobile receptors is 82.76 ± 0.66%. The remaining integrin population (17.24 ± 0.66%) is comprised of the mobile receptors, migrating from periphery to the middle. Some of them, however, are fast receptors, with velocity constant $(1/k_1) = 0.031 \pm 0.0017$, and the rest are slow receptors, having a velocity constant $(1/k_2) = 0.01 \pm 0.0012$. Using directly-measured velocities of particles in PZ and the ratio $D_1/D_2 = 3.143$, we can calculate that the quantity of fast receptors is greater than three-times that of slow receptors on glass (i.e., 13.08 ± 1.04% as fast and 4.16 ± 0.47% as slow receptors; see Table 3).

Conversely, the kinetics of integrin movement in the PZ on hydrophobic ODS (see Fig. 2 *A*, *circles*) fitted best to an exponential decay of first order,

$$D(t) = D_{min} + D_1 \times \exp^{(-t/k1)}. \quad (14)$$

Calculations yielded values of $D_{min} = 0.277 \pm 0.002$, $D_1 = 0.089 \pm 0.0045$, and $k_1 = 43.1 \pm 4.87$, suggesting the existence of only two receptor fractions: 1), immobile, with an approximate ratio of 83.36 ± 0.6%; and 2), mobile (i.e., the remaining), with a ratio of 16.640.6% (see Table 3).

TABLE 3 Relative quantity of different receptor populations in percentage of all integrins and their respective speeds in μm/min in the peripheral zone (PZ) of cells on glass and ODS, respectively

Parameter	Immobilized	Fast	Slow
Quantity (glass) (in % of all)	82.76 ± 0.70	13.08 ± 1.04	4.16 ± 0.47
Quantity (ODS) (in % of all)	83.36 ± 0.60	16.64 ± 0.60	Absent
Speed (glass) (in μm/min)	0	0.353 ± 0.020	0.114 (calculated)
Speed (ODS) (in μm/min)	0	0.211 ± 0.016	Absent

Therefore, the speed of the latter must be equal to that measured directly at 0.218 ± 0.02 μm/min (see Table 1). Turning back to the cell on glass, the speed of fast receptors must again be equal to the directly measured value of 0.353 ± 0.02 μm/min. From Eq. 13, however, we know the ratio of the velocity constants $1/k_1$ and $1/k_2$, and can easily calculate the speed of slow receptors as 0.114 ± 0.007 μm/min. Quantitative analysis at the MZ demonstrated a slight tendency for a decrease in the integrin density on glass, of ~3.8%. In contrast, on ODS, this density increased with 6.86%, probably resulting from movement of integrins from the PZ (Fig. 2 *B*). The density in the NZ on glass (Fig. 2 *C*), however, increased linearly with ~8.3% during the time of investigation, demonstrating some drifting of integrins from the middle region, whereas on ODS, the density remained constant.

DISCUSSION

Despite the fact that most of the information on matrix adhesion structures is based on static immunofluorescence images, it was always known that these sites are, in fact, dynamic, and that integrins play a crucial role for this. In fibroblasts, integrin dynamics is manifested by their assembly, disassembly, and translocation, which occur during cell spreading, polarization, and migration (30). Recently, the application of techniques for tagging of receptors with fluorescent protein or specific antibodies has facilitated studies on integrin dynamics. GFP-β_1-integrin fusion proteins have been recently applied to follow focal contacts dynamics in stationary fibroblasts (13), as well as the dynamics of GFP-α_5-integrin in moving CHO cells (18). In these investigations, it was observed, with some surprise, that integrins undergo a centripetal movement in both nonmotile and motile cells. Studies of Pankov et al. (12) are consistent with this observation, and have further shown that some of the antibody-bound $\alpha_5\beta_1$-integrins segregate from the focal contacts forming fibrillar adhesions. We assume that the velocities of integrin particles that we measured directly (see Table 1) actually represent the fast receptors' population. In our study the calculated rate of slow receptors with 0.114 ± 0.007 μm/min is very close to the rates obtained independently by Smilenov et al. (13) for moving focal contacts (0.12 ± 0.08 μm/min) and by Pankov et al. (12) for fibrillar adhesions (0.108 ± 0.012 μm/min). In comparison, the average rate of retrograde flow of α_5-integrins in CHO cells measured by Wiseman et al. (18) is ~0.29 μm/min.

There are many indications that the observed movements of β_1-integrins are instrumental for FN fibrillogenesis (12,30). Previously, we had also studied the organization of β_1-integrins on the dorsal cell surface of living fibroblasts using specific antibody tags and, for the first time to our knowledge, monitored their specific linear organization (31). In a further study, we showed that hydrophobic substrata affect the behavior of β_1-integrins significantly, and block their linear organization (29), which corroborates with the absence of FN matrix formation on those substrata (25,28). However, these observations were based on morphological examinations using fixed preparations that needed to be quantified with living cells. Here we applied an approach similar to that of Pankov et al. (12), using directly-labeled integrin antibodies. We expected, initially, that our experimental conditions (staining only for 10 min at 4°C) would highly restrict the binding of antibody to the ventral cell surface, for the reason of simple diffusion. In fact, we found sufficient fluorescent signal from the cells, assuming that we observe the behavior of integrins mainly on the dorsal cell surface. However, the existence of fast and slow receptor populations, as well as the relatively good coincidence between the theoretically calculated velocity of slow receptors and the velocities of the adhesive structures measured by other authors on the ventral cell surface (discussed above), indicate, presumably, that we monitor the integrin dynamics on both dorsal (fast population) and ventral (slow population) cell surfaces.

The movement of antibody-tagged β_1-integrins was not chaotic, and it was directed from the periphery to the center of the cell (i.e., centripetally). Similar translocation of both fibrillar adhesions and focal contacts were shown to be driven by actomyosin contractility (14). By analogy, therefore, we expect that the behavior of fast integrins on the dorsal cell surface may also be attributed to the *trans*-membrane association with the cytoskeleton and forces generated by the actin-myosin complex (32–34). Nevertheless, the latter mechanism still remains to be proved, as we did not block the centripetal movement of integrins with Y-27632, an inhibitor of the myosin light-chain activity (unpublished data). Considering that such *trans*-membrane association of integrins would need a proper transfer of signal via tyrosine phosphorylation, we looked for a possible co-localization of these dynamic structures with focal adhesion kinase (FAK) activity. We have to admit, however, that live-cell monitoring of FAK phosphorylation did not confirm such an event, and was later attributed mainly to the focal adhesions (35), as also shown by the measuring of FAK-Y397 and FAK-Y861 activity on fixed preparations (7). Moreover, FAK activity was not found in moving structures such as fibrillar adhesions (6,12). Thus, the mechanism of centripetal movement of β_1-integrins still remains unclear.

The direct measurement of the velocities of integrin-antibody clusters at different zones of the cell clearly distinguish the higher velocity of integrins on hydrophilic substrate in comparison to the hydrophobic ODS. Hence, with this approach, we provide for the first time, to our knowledge, quantitative data confirming the dependence of integrin behavior on substratum properties. We further found a zone-dependent difference in the integrin velocities. On glass, integrin velocity was higher in the middle zone of the cells, a fact that may be attributed to the absence of stable focal contacts in comparison to the peripheral zone. Conversely, at the cell periphery, we found lowered speed of β_1-integrins

on ODS, which may be explained by the stronger FN-to-substrate interaction (36,37). Many authors proposed that the centripetal movement is a part of the endocytic pathway connected with the degradation and recycling of integrins (31,38–41). The rearrangement of activated integrins to the adhesive site of the cell also involves the centripetal flow (17,42). Pankov et al. (12) and Katz et al. (6) suggest that the coordinated translocation of $\alpha_5\beta_1$ is presumably tightly connected with FN fibrillogenesis. Thus, one reason for the obtained quantitative difference in integrin behavior could be the inability of cells to generate FN fibrils on hydrophobic substrata (28), a process requiring tension (2); presumably, integrins here are less effective as mechanosensors (2,43). This effect could be also attributed to the altered signaling of β_1-integrins in focal adhesions, as we suggested previously (25), but also to the stronger substratum interaction of FN on hydrophobic substrata (5,36,44). Note that, on the latter surface, the slow receptor population, which provides a corroboration with the blocked adsorbed FN reorganization, was absent (28,37). We did not measure the generation of FN fibrils on the dorsal cell surface of living cells within the timeframe of experiment. When we treated them with antibody, the cells looked dark on the bright fluorescent background of adsorbed FN (not shown). However, it was not the case when we studied FN on the ventral cell surface, particularly on glass. When fibroblasts were fixed and permeabilized and then stained with Abs, initial FN fibrils were observed, as shown previously (26). Nevertheless, on hydrophobic ODS, such substratum-associated FN fibrils were absent (3,26), which again correlates with the absence of slow receptor population.

Finally, in the nuclear zone, on both hydrophilic and hydrophobic substrata, the centripetal movement of integrins was absent and receptor clusters here were found to turn around the nucleus, mostly on ODS. Some authors suggested the presence of a locus for regulation of cell motility located at the central region of the cell (17,45), and it is notable that, in this region, we observed the rotation of the integrins. Why it was especially pronounced on ODS, where the angular movement was many times higher than on glass? To our knowledge, such different behavior of integrins has never been reported previously, and obviously needs further attention. At this stage, we can only speculate that the stretching of the actomyosin fibrils is stronger at the cell rear, as they insert in focal adhesions that are more functional on glass. Moreover, this stretching orients the fibrils linearly, whereas on hydrophobic substrata this process is abrogated from the lowered signaling of integrins (3). Thus, in the middle of the cell, these integrins receive fewer sufficient support points, and therefore start spinning around the cell center.

Another novelty in this work was our approach to analyze the β_1-integrin densities at different zones of the cell. Here we could identify three populations of integrins on glass (i.e., immobilized, fast, and slow) and two on ODS (i.e., immobilized and fast). Surprisingly, the part of immobilized integrins on both surfaces was approximately equal ($\approx$83%). These are, presumably, the integrins located in focal contacts, as their ratio was very close to the ratios of immobilized integrins reported by Duband et al. (16) of 84% and Palecek et al. (17) of 80%. Our results corroborate also with the recent findings of Wiseman et al. (18), showing similar three populations of α_5-integrins (termed diffusing, flowing, and immobile) in migrating CHO B2 cells. Interestingly, the average part of immobile receptors (GFP-α_5-integrin) was $\sim$81% vs. 82.76% measured in our experiments. Conversely, the amount of diffusing and flowing receptors shows rather high dispersion, ranging from of 13–53% and 3–20%, respectively, but the ratio of their average values is surprisingly the same (3:1) as the ratio of fast to slow receptors in our experiments on glass.

The slow receptors defined in this article, we believe, are the moving focal adhesions on the ventral cell surface (13), which were stained less efficiently at our conditions and therefore their proportion was smaller (4.16%). Conversely, the fast receptors (13.08%) that we propose are localized on the dorsal cell surface presumably were not investigated up to now. The results showing their different behavior depending on the substratum properties are extremely interesting, as they represent β_1-integrin population that is not involved in the adhesion process. This suggests the existence of some common cellular mechanisms that control integrin dynamics in a substratum-dependent manner. In summary, we propose that the quantification of integrin dynamics can be applied as an additional tool for studying the complex process of cell-substratum interactions.

SUPPLEMENTARY MATERIAL

One can download a supplementary file as a video clip, demonstrating the integrin dynamics on a hydrophilic glass at: http://www.bio21.bas.bg/ibf/dpb_files/iz/Supplement1.avi and on hydrophobic ODS at: http://www.bio21.bas.bg/ibf/dpb_files/iz/Supplement2.avi. The minute mark of the scan (see Materials and Methods) is marked at the below-right corner of each image; the bar represents 20 μm.

Mrs. Ruth Hesse is acknowledged for technical assistance.

This work was supported by grants from Deutsche Forschungsgemeinschaft and GKSS Forschungszentrum to I.Z., and from the Marie Curie Program of the European Communities to G.A. Further financial support was obtained from the Bulgarian Science Foundation.

REFERENCES

1. Hynes, R. 1992. Integrins: versatility, modulation and signaling in cell adhesion. *Cell.* 69:11–25.
2. Geiger, B. A., A. Bershadsky, R. Pankov, and K. Yamada. 2001. Transmembrane extracellular matrix—cytoskeleton crosstalk. *Nat. Rev. Mol. Cell Biol.* 2:793–805.
3. Groth, T., and G. Altankov. 1998. Cell-surface interactions and the tissue compatibility of biomaterials. *In* New Biomedical Materials. P. Harris and D. Chapman, editors. IOS Press, Amsterdam. 12–23.

4. Webb, K., V. Hlady, and P. A. Tresco. 2000. Relationships among cell attachment, spreading, cytoskeletal organization and migration rate for anchorage-dependent cells on model surfaces. *J. Biomed. Mater. Res.* 49:362–368.
5. Grinnell, F. 1987. Fibronectin adsorption on material surfaces. *In* Blood in Contact with Natural and Artificial Surfaces. *Ann. N. Y. Acad. Sci.* 516:280–290.
6. Katz, B.-Z., E. Zamir, A. Bershadsky, Z. Kam, K. Yamada, and B. Geiger. 2000. Physical state of the extracellular matrix regulates the structure and molecular composition of cell-matrix adhesions. *Mol. Biol. Cell.* 11:1047–1060.
7. Keselowsky, B. G., D. M. Kollard, and A. D. Garcia. 2004. Surface chemistry modulates focal adhesion composition and signaling through changes in integrin binding. *Biomaterials.* 25:5947–5954.
8. Izzard, C. S., and L. R. Lochner. 1976. Cell-to-substrate contacts in living fibroblasts: an interference reflection study with an evaluation of the technique. *J. Cell Sci.* 21:129–159.
9. Burridge, K., T. Fath, G. Kelly, G. Nuckolls, and C. Turner. 1988. Focal adhesions: transmembrane junctions between the extracellular matrix and the cytoskeleton. *Annu. Rev. Cell Biol.* 4:487–525.
10. Chen, W. T., and S. J. Singer. 1982. Immunoelectron microscopic studies of the sites of cell-substratum and cell-cell contacts in cultured fibroblasts. *J. Cell Biol.* 95:205–222.
11. Zamir, E., B.-Z. Katz, S. Aota, K. M. Yamada, B. Geiger, and Z. Kam. 1999. Molecular diversity of cell-matrix adhesions. *J. Cell Sci.* 112: 1655–1669.
12. Pankov, R., E. Cukierman, B.-Z. Katz, K. Matsumoto, D. Lin, S. Lin, C. Hahn, and K. Yamada. 2000. Integrin dynamics and matrix assembly: tensin-dependent translocation of $\alpha5\beta1$-integrins promotes early fibronectin fibrillogenesis. *J. Cell Biol.* 148:1075–1090.
13. Smilenov, L., A. Mikhailov, R. Pelham, Jr., E. Marcantonio, and G. Gundersen. 1999. Focal adhesion motility revealed in stationary fibroblasts. *Science.* 286:1172–1174.
14. Zamir, E., M. Katz, Y. Posen, N. Erez, K. M. Yamada, B.-Z. Katz, S. Lin, D. C. Lin, A. Bershadsky, Z. Kam, and B. Geiger. 2000. Dynamics and segregation of cell-matrix adhesions in cultured fibroblasts. *Nat. Cell Biol.* 2:191–196.
15. Petit, V., and J.-P. Thiery. 2000. Focal adhesions: structure and dynamics. *Biol. Cell.* 94:477–494.
16. Duband, J.-L., G. Nuckolls, A. Ishihara, T. Hasegawa, K. Yamada, J.-P. Thiery, and K. Jacobson. 1988. Fibronectin receptor exhibits high lateral mobility in embryonic locomoting cells but is immobile in focal contacts and fibrillar streaks in stationary cells. *J. Cell Biol.* 107:1385–1396.
17. Palecek, S., C. Schmidt, D. Lauffenburger, and A. Horwitz. 1996. Integrin dynamics on the tail region of migrating fibroblasts. *J. Cell Sci.* 109:941–952.
18. Wiseman, P. W., C. M. Brown, D. J. Webb, B. Hebert, N. L. Johnson, J. A. Squier, M. H. Ellisman, and A. F. Horwitz. 2004. Spatial mapping of integrin interactions and dynamics during cell migration by image correlation microscopy. *J. Cell Sci.* 117:5521–5534.
19. Kawakami, K., H. Tatsumi, and M. Sokabe. 2001. Dynamics of integrin clustering at focal contacts of endothelial cells studied by multimode imaging microscopy. *J. Cell Sci.* 114:3125–3135.
20. Miyamoto, S., S. K. Akiyama, and K. Yamada. 1995. Synergistic roles for receptor occupancy and aggregation in integrin transmembrane function. *Science.* 267:883–885.
21. Miyamoto, S., H. Teramoto, O. A. Coso, J. S. Gutkind, P. D. Burbelo, S. K. Akiyama, and K. M. Yamada. 1995. Integrin function: molecular hierarchies of cytoskeletal and signaling molecules. *J. Cell Biol.* 131: 791–805.
22. Arroyo, A. G., A. Garcia-Pardo, and F. Sanchez-Madrid. 1993. A high affinity conformational state on VLA integrin heterodimers induced by an anti-β_1 chain monoclonal antibody. *J. Biol. Chem.* 268:9863–9868.
23. Mould, A. P., A. N. Garratt, J. A. Askari, S. K. Akiyama, and M. J. Humphries. 1995. Identification of a novel anti-integrin mAb that recognizes a ligand-induced binding site epitope on the $\beta1$ subunit. *FEBS Lett.* 363:118–122.
24. Cruz, M. T., C. L. Dalgard, and M. J. Ignatius. 1997. Functional partitioning of β_1 integrins revealed by activating and inhibitory mAbs. *J. Cell Sci.* 110:2647–2659.
25. Groth, T., and G. Altankov. 1995. Fibroblast spreading and proliferation on hydrophobic and hydrophilic surfaces is related to tyrosine phosphorylation in focal contacts. *J. Biomater. Sci. Polymer E.* 7:297–305.
26. Altankov, G., and T. Groth. 1996. Fibronectin matrix formation and the biocompatibility of materials. *J. Mater. Sci. Mater. Med.* 7:425–429.
27. Groth, T., and G. Altankov. 1996. Studies on cell-biomaterial interaction: role of tyrosine phosphorylation during fibroblast spreading on surfaces varying in wettability. *Biomaterials.* 17:1227–1234.
28. Altankov, G., and T. Groth. 1994. Reorganization of substratum-bound fibronectin on hydrophilic and hydrophobic materials is related to biocompatibility. *J. Mater. Sci. Mater. Med.* 5:732–737.
29. Altankov, G., T. Groth, N. Krasteva, W. Albrecht, and D. Paul. 1997. Morphological evidence for a different fibronectin receptor organization and function during fibroblast adhesion on hydrophilic and hydrophobic glass substrata. *J. Biomater. Sci. Polymer E.* 8:721–740.
30. Zamir, E., and B. Geiger. 2001. Molecular complexity and dynamics of cell-matrix adhesions. *J. Cell Sci.* 114:3583–3590.
31. Altankov, G., and F. Grinnell. 1995. Fibronectin receptor internalization and AP-2 complex reorganization in potassium-depleted fibroblasts. *Exp. Cell Res.* 216:1–11.
32. Giuliano, K. A., and D. L. Taylor. 1995. Measurement and manipulation of cytoskeletal dynamics in living cells. *Curr. Opin. Cell Biol.* 7: 4–12.
33. Galbraith, C. G., and M. P. Sheetz. 1997. A micromachined device provides a new bend on fibroblast traction forces. *Proc. Natl. Acad. Sci. USA.* 94:9114–9118.
34. Galbraith, C. G., and M. P. Sheetz. 1998. Forces on adhesive contacts affect cell function. *Curr. Opin. Cell Biol.* 10:566–571.
35. Kirchner, J., Z. Kam, G. Tzur, A. D. Bershadsky, and B. Geiger. 2003. Live-cell monitoring of tyrosine phosphorylation in focal adhesions following microtubule disruption. *J. Cell Sci.* 116:975–986.
36. Grinnell, F., and M. K. Feld. 1981. Adsorption characteristics of plasma fibronectin in relationship to biological activity. *J. Biomed. Mater. Res.* 15:363–381.
37. Altankov, G., F. Grinnell, and T. Groth. 1996. Studies on the biocompatibility of materials: fibroblast reorganization of substratum-bound fibronectin on surfaces varying in wettability. *J. Biomed. Res.* 30:385–391.
38. Bretscher, M. S. 1989. Endocytosis and recycling of the fibronectin receptor in CHO cells. *EMBO J.* 8:1341–1348.
39. Watts, C., and M. Marsh. 1992. Endocytosis: what goes in and how? *J. Cell Sci.* 103:1–8.
40. Sczekan, M. M., and R. L. Juliano. 1990. Internalization of the fibronectin receptor is a constitutive process. *J. Cell. Physiol.* 142:574–580.
41. Tawil, N., P. Wilson, and S. Carbonetto. 1993. Integrins in point contacts mediate cell spreading—factors that regulate integrin accumulation in point contacts vs. focal contacts. *J. Cell Biol.* 120:261–271.
42. Lawson, M. A., and F. R. Maxfield. 1995. Ca^{2+}- and calcineurin-dependent recycling of an integrin to the front of migrating neutrophils. *Nature.* 377:75–79.
43. Riveline, D., E. Zamir, N. Q. Balaban, U. S. Schwarz, T. Ishizaki, S. Narumiya, Z. Kam, B. Geiger, and A. D. Bershadsky. 2001. Focal contacts as mechanosensors: externally applied local mechanical force induces growth of focal contacts by an mDia1-dependent and ROCK-independent mechanism. *J. Cell Biol.* 153:1175–1186.
44. Andrade, J. D., and V. Hlady. 1986. Protein adsorption and materials biocompatibility. A tutorial review and suggested hypothesis. *Prog. Surf. Sci.* 79:1–64.
45. Ballestrem, C., Z. Hinz, B. A. Imhof, and B. Wehrle-Haller. 2001. Marching at the front and dragging behind: differential $\alpha_v\beta_3$-integrin turnover regulates focal adhesion behavior. *J. Cell Biol.* 155:1319–1332.